Received: 23 December 2021 | Revised: 1 March 2022 | Accepted: 18 March 2022

DOI: 10.1096/fba.2021-00166

FASEB BioAdvances WILEY

RESEARCH ARTICLE

Human iPSC colon organoid function is improved by exposure to fecal fermentates

Sarah C. Pearce[1] | **Gregory J. Weber**[1] | **Laurel A. Doherty**[2] | **Jason W. Soares**[2]

[1]Soldier Sustainment Directorate, Combat Capabilities Development Command Soldier Center, Natick, Massachusetts, USA

[2]Soldier Effectiveness Directorate, Combat Capabilities Development Command Soldier Center, Natick, Massachusetts, USA

Correspondence
Sarah C. Pearce, 1015 N. University Blvd, Ames, IA 50011, USA.
Email: sarah.pearce@usda.gov

Present address
USDA-ARS National Laboratory for Agriculture and the Environment, Ames, Iowa, USA

Funding information
Department of Defense Combat Feeding Research and Engineering Program project "Gut Microbiome and Performance Nutrition" and The Applied Research for the Advancement of Science and Technology Priorities (ARAP) Program on Synthetic Biology for Military Environments (SBME), funded by the Office of the Secretary of Defense.

Abstract

The host–microbe interaction is critical for intestinal homeostasis. By-products from microbial metabolism of unabsorbed dietary components have been studied increasingly as potential contributors to health and disease. In vitro fermentation systems provide a way to simulate microbial activity and by-product production of the colon using human fecal samples. Objectives of the study were to determine how clarified supernatants from two different fermentation conditions affect markers of cell proliferation, differentiation, barrier function, and immune function in a human-induced pluripotent (iPSC) colon organoid model. SCFA and BCFA's of the supernatants were analyzed and were similar to known in vivo concentrations. Molecular results showed 25% of the clarified supernatant from batch fermentation led to a more physiological intestinal phenotype including increased markers of differentiation, including alkaline phosphatase, chromogranin A, SCFA transport monocarboxylate transporter-1, (6.2-fold, 2.1-fold, and 1.8-fold, respectively; $p < 0.05$). Mucin production (mucin-2, mucin-4) was increased in cells treated with 25% supernatant, as observed by confocal microscopy. In addition, increased tight junction expression (claudin-3) was noted by immunofluorescence in 25% supernatant- treated cells. A dose–response increase in barrier function was observed over the 72-h time course, with a twofold increase in transepithelial electrical resistance (TER) in the 25% group compared to the control group ($p < 0.05$). To further investigate host effects, clarified supernatants from a continuous multistage fermentation representing the ascending (AC), transverse (TC), and descending (DC) colonic domains were utilized and some regional differences were observed including increased markers of inflammation (IL-1β, 6.15 pg/ml; IL-6, 27.58 pg/ml; TNFα, 4.49 pg/ml; $p < 0.05$) in DC-treated samples only. Overall, clarified supernatants represent a valuable model to examine effects of microbial by-products on host intestinal development and function

Abbreviations: AC, ascending colonBCFAbranch-chain fatty acidsBFbatch fermentationCFcontinuousDCdescending colonFSfecal supernatantHEPES(4-(2-hydroxyethyl)-1-piperazineethanesulfonic acidiPSCinduced pluripotent stem celljA^{2}COBjoint army colon on a benchTCtransverse colonTERtransepithelial electrical resistanceSCFAshort-chain fatty acid.

and future efforts will be designed to further understand microbial communities and metabolites, along with additional host response measures.

KEYWORDS
differentiation, fermentation, metabolites, organoids

1 | INTRODUCTION

The intestinal-microbiome interface is a complex and intricate network that facilitates the breakdown of dietary nutrients by microbes, resulting in metabolites that can interact with, or cross the epithelial barrier.[1] These interactions stimulate the intestinal, immune, and nervous systems resulting in systemic signaling to the host and potential crosstalk between the host and microbes. However, study of this interaction can be quite difficult. The use of in vitro fermentation models allows for study of microbial metabolism and derived metabolites as a function of nutritional inputs or media supplementation to simulate specific sections of the digestive tract. In vitro fermentation models range in complexity from single-stage batch fermentation systems to continuous culture systems with multiple connecting stages representing different colonic domains.[2–4]

The host–Microbe interaction is especially critical when discussing the epithelial barrier and specifically the mucin layer of the colon, which provides a first level defense against microbes. The colonic mucosa consists of two mucin layers and a glycocalyx which is adhered to the epithelium. Secondarily, the epithelial barrier between cells provides another defense mechanism, and cells which reside there produce antimicrobial and immune response agents.[5] Host–microbe or host-metabolite interaction studies in real time have been difficult, although newer research tools including organ-on-a-chip technology consisting of primary cell culture models have made large strides in creating more physiologically relevant models.[6] Our group has been utilizing more physiologically relevant intestinal organoid models, which recapitulate in vivo intestinal cell types and function, to examine effects of short-chain fatty acids (SCFA's)[7] and other nutrients/metabolites on the intestinal epithelium.[5,8,9] We and others have optimized the usage of intestinal organoid monolayers that create a polarized epithelium to study intestinal barrier properties and nutrient interactions more effectively.[10,11] In addition, induced pluripotent stem cell (iPSC) models of the intestine have become increasingly popular for a multitude of research areas.[12,13]

This study utilizes a custom designed in vitro fermentation model of the large intestine, the "joint Army Automated Colon on a Bench" (jA^{2}COB).[12] The simulated large intestine model is seeded with human fecal samples for both batch fermentation in single colonic domain mode and continuous multistage fermentations simulating transit through multiple domains under domain-specific parameters. Clarified fecal supernatants (FS) derived from this model, combined with human intestinal organoids were used to examine bacterial metabolite-driven epithelial differentiation, with primary focus on host response using a commercially available undifferentiated iPSC colon organoid model. Our overall objective for this study was to elucidate how *in vitro*-derived clarified FS from two different fermentation conditions alter intestinal cell function in a human iPSC colon cell line with emphasis on model development and characterization. Specific objectives were to elucidate effects on intestinal barrier function, differentiation, mucin formation, and immune response. This synergistic model allows for assessment of intestinal cell physiology as a function of microbial-derived fermentation by-products and can be used for future evaluation of nutritional interventions and stressors as we build toward a fully integrated model incorporating complex intestinal epithelia with an immune system, as well as live microbiota. Integrating in vitro fermentation with human organoid models provides a useful and effective tool to study clarified supernatant responses on the host.

2 | MATERIALS AND METHODS

2.1 | Organoids

Commercially available integration-free human-induced pluripotent stem cells (3dGRO Human iPSC Derived Colon Organoids) from the colon were utilized. (Cat #SCC300, Sigma Aldrich) adhering to company guidelines for research usage. For characterization comparison purposes only, healthy biopsy-derived colon organoids from the distal colon were utilized (source, Harvard Digestive Disease Center) from a de-identified tissue source.

2.2 | 3D cultures

As previously described by our group,[7] frozen organoids were thawed and immediately transferred to a 15-ml conical tube with 5 ml of Advanced DMEM/F12, 0.2 mM Glutamax, and 10 mM HEPES. Cells were then gently

spun down at 300× g for 10 min and supernatant removed. Organoid pellets were resuspended in growth-factor reduced Matrigel (#356231, Corning). Aliquots (40 µl) containing ~100 organoids were plated in individual wells of a 24-well tissue culture treated plate and incubated at 37°C for 10 min before adding 0.5 ml of media (3DGRO Human Colon Organoid Expansion Medium; Sigma Aldrich). Media was replaced every 2 days, and organoids were passaged every 7–9 days by incubation in Gentle Cell Dissociation Reagent (Stem Cell Technologies) at 4°C with shaking for 40 min. Well contents were scraped and triturated with a P200 pipette tip 30–50 times to break apart organoids, collected in a 15-ml conical tube with 1:1 addition of DMEM/F12 media and centrifuged at 300 × g for 10 min. Cell pellets were resuspended in Matrigel to achieve a similar density each time. Three dimensional cultures were used to populate 2D monolayers.

2.3 | 2D monolayer cultures

Monolayer protocols were adapted from previous publications with minor modifications.[8] Differentiation media was not utilized in the study as we were interested in effects of FS on differentiation. Organoids were initially cultured in Matrigel for 2–3 passages prior to plating on monolayers. To form monolayers, Transwell inserts (24-well inserts, 0.33 cm^2 surface area, 0.4 µm pore polyester membrane; Corning) were coated with Human Collagen IV (Millipore Sigma) solution (final concentration of 10 µg/cm^2) and incubated overnight at 4°C. Prior to plating, any remaining collagen was removed from wells and washed 2X with Advanced DMEM/F12. Fragments for monolayer plating were obtained using the passaging protocol above, making sure to obtain small fragments. Approximately 50 organoid fragments were obtained per 100 µl Intesticult™ media (Stem Cell Technologies), then added to the membrane and allowed to settle at 37°C; 600 µl of media was also added to the basolateral side. Intesticult™ media was changed every 2 days and monolayer development was tracked using transepithelial electrical resistance (TER) measured by the EVOM2 epithelial voltohmmeter (World Precision Instruments). Monolayers were utilized for experiments when cells reached a minimum 400 Ω. Average baseline TER for all treatments was 575 Ω.

2.4 | In vitro fermentation

FS were generated from in vitro fecal fermentations as described in Pantoja et al.[14] with some modifications. An initial batch fermentation (BF) was held at pH 6.8 and sampled after 24 h; subsequently, a series of continuous multistage in vitro fermentations under conditions for the ascending (AC), transverse (TC), and descending (DC) colon were held at pH 5.5, 6,2, and 6.8, respectively, and were sampled after several days at steady state. Sample aliquots were centrifuged at 8000 × g for 10 min and passed through a 0.2-µm surfactant-free cellulose acetate syringe filter to remove microbial organisms, and stored at 4°C. Thus, all FS utilized were clarified and bacteria-free.

2.5 | Organoid treatment with FS

FS were diluted in Intesticult™ media prior to use to achieve desired concentration. For the first set of experiments, 2D organoids were apically treated for 72 h with either 1, 10, or 25% of batch fermentation supernatant (BF; representing the descending colon) diluted in cell media. For the second set of experiments, 2D organoids were apically treated for 72 h with 10% of continuous multistage FS diluted in cell media from the ascending (AC), transverse (TC), or descending (DC) colon. For both sets of experiments, controls (CON), were non-treated cells. At the end of the experiment, media was collected from the basolateral compartment for 2D and frozen at −80°C for later use. After media removal, cells were collected for either RNA extraction or total protein. For RNA collection, TRIzol (Life Technologies) was added to each well to suspend cells and aliquoted to a new 1.5 ml tube and frozen at −80°C for later extraction. Cells intended for total protein collection were resuspended in Gentle Dissociation Reagent (Stem Cell Technologies) and frozen at −80°C. Transepithelial electrical resistance (TER) was measured every 24 h by the EVOM2 epithelial voltohmmeter (World Precision Instruments).

2.6 | Short and branch-chain fatty acid extraction and analysis

SCFA and BCFA concentrations in in vitro FS samples were measured as previously described[15,16] with minor modifications. FS aliquots were thawed immediately prior to extraction, acidified using 50% sulfuric acid (H_2SO_4;2:1 v/v), and then fatty acids were extracted using diethyl ether (2:5 v/v). After incubating on ice for 2 min, samples were centrifuged (12,000 × g for 10 min at 4°C), the organic layer removed, and ethyl butyric acid was added as an internal standard. Samples were then stored at -80°C until analysis. Acetic acid, propionic acid, butyric acid, iso-butyric acid, and iso-valeric acid were quantified using an Agilent 7890A GC system with Flame Ionization

Detection (30 m × 250 μm, ×0.25 μm; DB-FFAP, Agilent J&W). Samples (1 μl) were injected by autosampler in duplicate using a split ratio of 10:1. The temperature program started at 110°C for 1 min, increased 15°C/min up to 180°C, and was then maintained at 180°C for 1 min. The carrier gas was nitrogen with a constant flow of 1 ml/min. Calibration standards (Sigma Aldrich) were included for each fatty acid and used for peak identification and quantification.

2.7 | RNA extraction & mRNA analysis

Total RNA was extracted from the TRIzol™ reagent-intestinal organoid solution combined with a commercially available spin-column kit (RNeasy Micro, Qiagen, Hilden Germany). Chloroform was added to samples in TRIzol™ and then samples were spun down at 15,000 × g for 15 min. The resulting supernatant was then transferred to a new tube and equal volumes of 70% ethanol were added. Samples were then transferred to spin columns and kit protocol was followed. Next, cDNA was synthesized using the Maxima First Strand cDNA Synthesis Kit (ThermoFisher Scientific). Real-time polymerase chain reaction using a BioRad CFX Connect was used to analyze mRNA expression using Maxima SYBR green (ThermoFisher Scientific). Data were analyzed using the Delta–Delta Ct ($2^{-\Delta\Delta Ct}$) method and presented as relative fold gene expression. Treatments were all made relative to controls, which were set to equal one. All samples were standardized to 18S expression as a housekeeping gene, and 18S values were determined to be statistically similar between treatment groups ($p > 0.05$). β-actin, RPL32, and 18S were tested prior to choosing an adequate housekeeping gene and 18S was chosen due to stability. Primer sequences are listed in Table S1.

2.8 | Immunofluorescence staining

Monolayers (2D) were grown on Transwell inserts prior to staining. Organoids in both conditions were fixed in 10% ice-cold acetone for 15 mins with no permeabilization step required. Organoids were then stained with tight junction proteins claudin-3 (CLDN3; Abcam), claudin-7 (CLDN7; ThermoFisher Scientific), zonula occludens-1 (ZO1; Abcam, Cambridge, MA), occludin (OCLN; Thermofisher Scientific), mucin-2 (MUC2; Abcam, Waltham MA), mucin-4 (MUC4; Abcam), and caspase-1 (CASP1; Proteintech) overnight at 4°C with secondary antibody incubation 1 h at 25°C. For characterization, iPSC and human biopsy-derived organoids were stained with vimentin (VIM; Abcam) and forkhead box F1 (FOXF1; Abcam). Nuclei were stained with 4′,6-diamidino-2-phenylindole (DAPI; Sigma Aldrich). Samples were mounted with coverslips containing ProLong Gold Antifade Mounting medium (ThermoFisher Scientific). Confocal images were obtained on a Zeiss LSM 710 upright confocal microscope. Images were acquired with Zen Software Version 3.3 (Zeiss; Oberkochen, Germany, https://www.zeiss.com/microscopy/int/products/microscope-software.html) as Z-stack and then rendered in 3D for final images. To image mucus accumulation and thickness, mucus height and area were analyzed in the z-plane of monolayers using ImageJ software. Images of cells exposed to different treatments were taken with the same settings and on the same day. Fluorescence values correlated to protein expression were analyzed using the corrected total cell fluorescence (CTCF) method where CTCF = Integrated Density−−(Area of selected marker x mean fluorescence of the background) and then made relative to controls (CON) so that CON = 1.0. Calculations were based on MUC2 and MUC4 monolayers separately (ImageJ version 1.8, NIH, https://imagej.nih.gov/ij/).

2.9 | Scanning electron microscopy (SEM)

Transwell membranes were aspirated and washed 2X with PBS for 5 min each. Cells were fixed in 2.5% glutaraldehyde in PBS for 7 min, then dehydrated in a graded ethanol series (25%, 50%, 70%, and 90%) for 7 min each prior to a final step in 100% (×3) for 5 min each. Membrane inserts were removed from the plate and transferred to a Tousimis 931 critical point dryer and dried under automatic system conditions. Dried membranes were adhered to standard aluminum SEM stubs with carbon tape and cut away from membrane holder. Membranes were then sputter coated for 180 s with a total deposit of 51 nm gold palladium. Finally, cells were imaged on a ThermoFisher Scientific Quattro Field Emission Environmental Scanning Electron Microscope (FE-ESEM) under high vacuum mode using an ETD secondary electron detector. Beam conditions were set to a voltage of 20 kV and spot size 2.0. Stage working distance was set to 10 mm. Images were acquired at 5 k and 20 k magnification across all sample conditions.

2.10 | Secreted protein analyses

Basolateral media from organoids cultured in 2D were analyzed for secreted proteins using a custom ProcartaPlex Immunoassay Kit with antibody-based magnetic beads (ThermoFisher Scientific) for the following targets:

interleukin 1β (IL-1β), interleukin-6 (IL-6), interleukin-10 (IL-10), interleukin-17A (IL-17A), interleukin-18 (IL-18), interleukin-21 (IL-21), interleukin 23 (IL-23), tumor necrosis factor-α (TNFα), interferon gamma (IFN-γ), cluster of differentiation 14 (CD14), regenerating islet-derived protein 3-α (REG3A), caspase-3 (CASP3), and monocyte chemoattractant protein-1 (MCP-1). Samples were read and fluorescent intensities were analyzed on a MAGPIX multiplexing system (Luminex, Northbrook, IL). Interleukin-8 (IL-8/CXCL8) was also analyzed using a commercially available sandwich ELISA kit (R&D Systems).

2.11 | Statistical analysis

Experiments were analyzed in JMP SAS (Version 9.2, SAS institute, https://www.jmp.com/en_us/home.html). Individual wells were used as technical replicates. Data were analyzed with a one-way ANOVA with the Tukey–Kramer adjustment for pairwise comparisons. Data are presented as least square means ± standard error of the mean. Means not sharing any letter are significantly different by the Tukey–Kramer test at $p < 0.05$.

3 | RESULTS

The human gut microbiome produces a wide array of fermentation by-products and other molecules, beneficial and otherwise, that impact and facilitate cross talk with host cells. By employing in vitro fermentation, a microbiome derived from human fecal samples was cultivated in the absence of host cells, but filtered fermentation culture supernatants still demonstrated an effect on host cell response in a colon organoid model.

3.1 | SCFA and BCFA analysis

As expected, the control media had little to no detectable SCFA, nor BCFA. The batch fecal supernatant (BF) had a total amount of SCFA's of 262.7 mM at approximately a 60:20:20 ratio of acetate:propionate:butyrate (Table 1). In the continuous multistage fermentation, acetate levels increased from 45.6 mM to 69.3 mM from ascending (AC) to descending (DC) colon. Propionate and valerate were also increased from 14.9 to 34.3 mM and 0.9 to 8.6 mM, respectively, while butyrate remained largely unaltered. Iso-butyrate and iso-valerate BCFA's increased from 0 to 4.9, and 0 to 6.9 mM, respectively (Table 1).

3.2 | Batch fermentation

3.2.1 | mRNA expression

To gauge the ability of bacterial metabolites to force undifferentiated stem cell organoid monolayers to differentiate, we analyzed mRNA expression of 18 genes total. Gene families included cell biomarkers and transporters, mucin dynamics, Toll-like receptors, and barrier function-related genes. Compared to controls (CON), stem cell biomarker *LGR5* was significantly reduced, regardless of percentage of FS ($p < 0.05$; Figure 1). Antimicrobial peptide lysozyme (*LYZ*) was significantly reduced at 25% FS ($p < 0.05$) as compared 1 and 10%. Conversely, enterocyte biomarker alkaline phosphatase (*ALPI*), enteroendocrine marker Chromogranin A (*CHGA*), and monocarboxylate transporter 1 (*MCT1*) were significantly elevated at 25% FS (6.2-fold, 2.1-fold, and 1.8-fold, respectively; $p < 0.05$) as compared to all other treatments. In the mucin gene

TABLE 1 Short and branch-chain fatty acid concentrations in human FS

	Concentration (mM)						
	Acetic	Propionic	Iso-Butyric	Butyric	Iso-Valeric	Valeric	Total
CON[a]	2.6 ± 0.1	0	0	0.3 ± 0.02	0	0	3.1 ± 0.1
Batch (BF)[b]	158.1 ± 5.7	53.3 ± 2.0	1.3 ± 0.1	46.3 ± 1.8	2.6 ± 0.1	1.1 ± 0.1	262.7 ± 1.6
Ascending (AC)[c]	45.6 ± 2.9	14.9 ± 1.0	0	77.1 ± 5.3	0	0.9 ± 0.1	138.4 ± 2.3
Transverse (TC)[c]	61.1 ± 5.0	31.8 ± 1.7	4.3 ± 0.2	78.9 ± 4.5	6.1 ± 0.3	2.4 ± 0.1	184.9 ± 2.0
Descending (DC)[c]	69.3 ± 3.8	34.3 ± 1.9	4.9 ± 0.3	78.4 ± 4.6	6.9 ± 0.4	8.6 ± 0.5	202.5 ± 1.9

[a]CON—control media, not containing fecal matter or bacteria.

[b]Pooled fecal samples underwent a batch fermentation method resembling descending colon.

[c]Pooled fecal samples underwent a continuous multistage fermentation method resembling specific colonic regions.

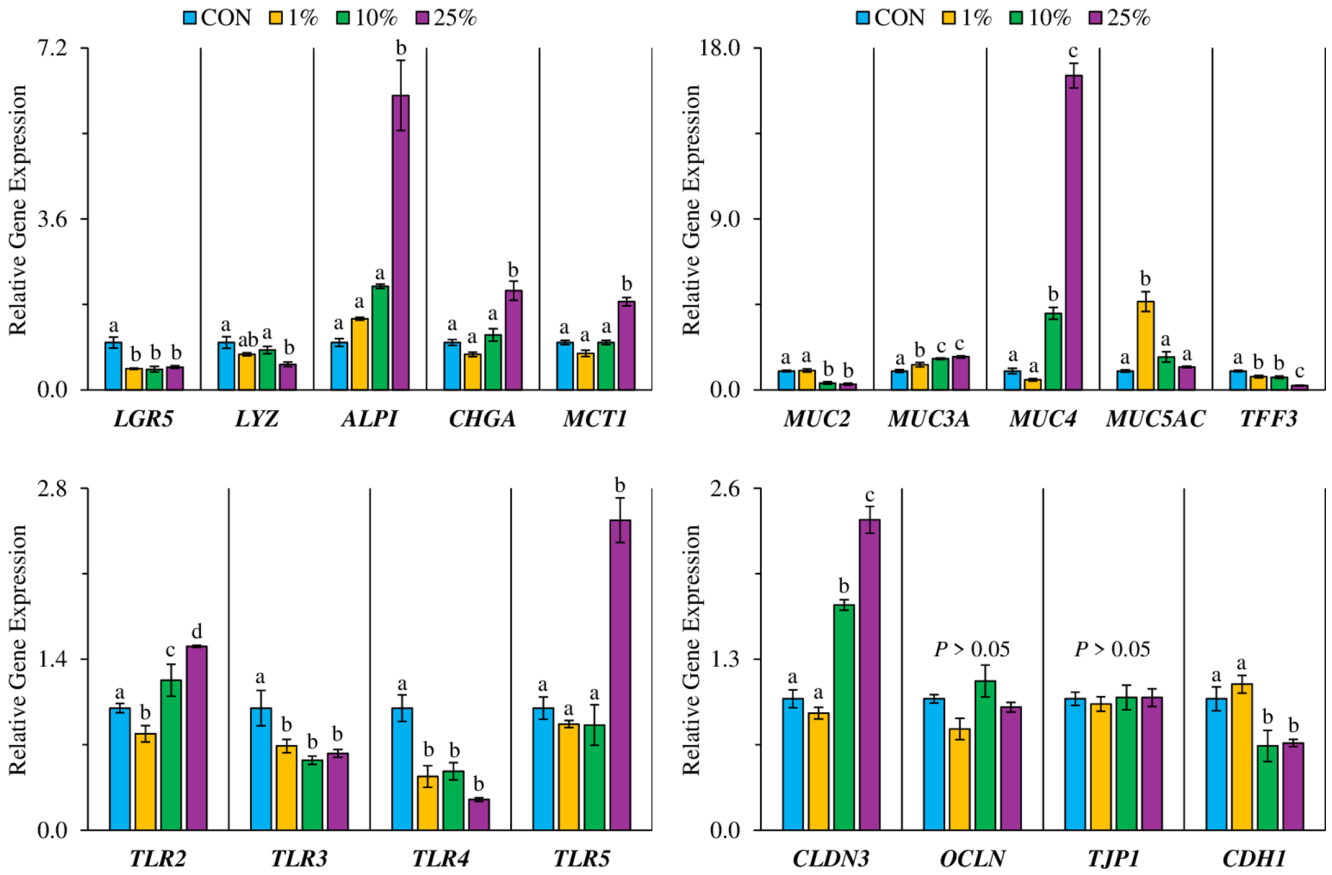

FIGURE 1 iPSC colon organoid monolayers were treated with 1%, 10%, or 25% batch fermentation supernatant (BF) for 72 h. mRNA expression of several markers including leucine-rich (*LGR5*), lysozyme (*LYZ*), alkaline phosphatase (*ALPI*), chromogranin A (*CHGA*), monocarboxylate transporter 1 (*MCT1*), mucin-2 (*MUC2*), mucin-3A (*MUC3A*), mucin-4 (*MUC4*), mucin-5 AC (*MUC5AC*), trefoil factor 3 (*TFF3*), Toll-like receptor 2 (*TLR2*), Toll-like receptor 3 (*TLR3*), Toll-like receptor 4 (*TLR4*), Toll-like receptor 5 (*TLR5*), claudin-3 (*CLDN3*), occludin (*OCLN*), tight junction protein 1 (*TJP1*), and cadherin 1 (*CDH1*) were analyzed and compared to controls which are set to 1.0. Different letters represent differences among treatments within each gene, $n = 6$

family, Mucin 2 (*MUC2*) expression was significantly downregulated at 10 and 25% compared to CON, conversely *MUC3A* and *MUC4* were significantly upregulated at 10 and 25% (1.7-fold and 16-fold, respectively at 25%; $p < 0.05$) relative to CON. *MUC5AC* was only significantly increased at 1% FS compared to all other treatment groups ($p < 0.05$). Trefoil factor 3 (*TFF3*) was significantly decreased by all FS treatments with the largest effects observed at 25% FS ($p < 0.05$). All toll-like receptors (TLR) analyzed were significantly altered with FS treatment. Interestingly, *TLR2* and *TLR5* were upregulated at 25% FS compared to all other treatments while *TLR3* and *TLR4* were decreased at all FS percentages as compared to CON ($p < 0.05$). In the barrier function gene family, claudin 3 (*CLDN3*) expression was significantly elevated at 10 and 25% compared to CON (1.7 and 2.4-fold, respectively; $p < 0.05$) while cadherin 1 (*CDH1*) expression was significantly decreased at 10 and 25% as compared to CON ($p < 0.05$). However, gene expression of occludin (*OCLN*) and tight junction protein 1 (*TJP1*) were not altered due to treatment ($p > 0.05$).

3.2.2 | Immunofluorescence

Supernatant from batch fermentation elicited increased relative fluoresence of zonula occludens-1 (ZO1), occludin (OCLN), and claudin 3 (CLDN3) as determined by corrected immunofluorescent intensity at 10% and 25% FS treatment ($p < 0.05$; Figure 2). An additional TJ protein, Claudin-7 (CLDN7) also appeared to follow a similar trend to CLDN3 (Figure S3A). Secreted mucin MUC2 and adherent mucin, MUC4 protein expression as measured by immunofluorescence indicated presence of both mucin types (Figure 3). Cells treated with higher concentrations of FS formed a > 20 μM thick layer of apical mucus. Mucin thickness as measured in both MUC2 and MUC4 monolayers was increased at 10 and 25% compared to CON and 1% BF treatment (1.6-fold; $p < 0.05$; Table 2) but there were

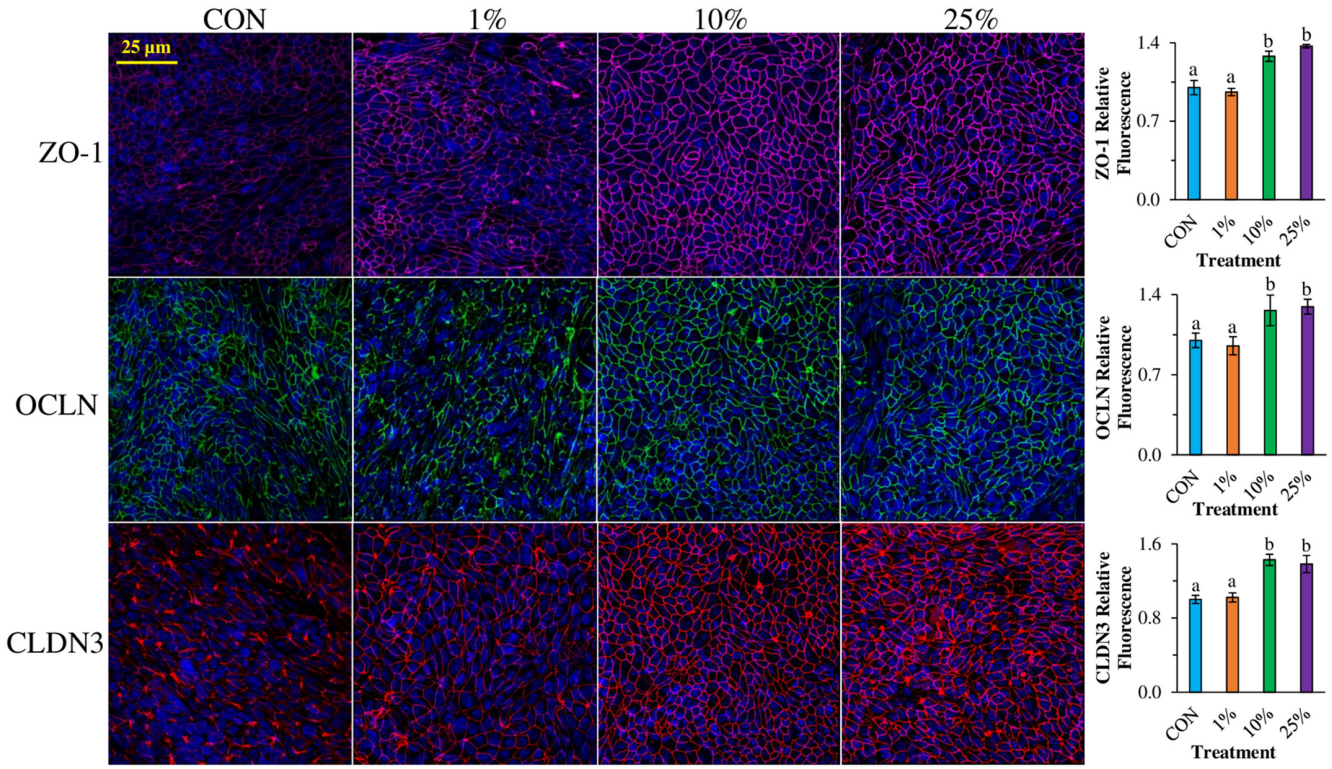

FIGURE 2 iPSC colon organoid monolayers were treated with 1%, 10%, or 25% batch fermentation supernatant (BF) for 72 h. Tight junction proteins zonula occluden 1 (ZO-1; magenta), occludin (OCLN; green), and claudin 3 (CLDN3; red) were analyzed and relative fluorescent intensity calculated. Nuclei are stained with DAPI (blue). Images are representative fields of view at 40X magnification. Different letters represent differences among treatments, $n = 6$. Images were obtained with Zen Software Version 3.3 (Zeiss; Oberkochen, Germany, https://www.zeiss.com/microscopy/int/products/microscope-software.html)

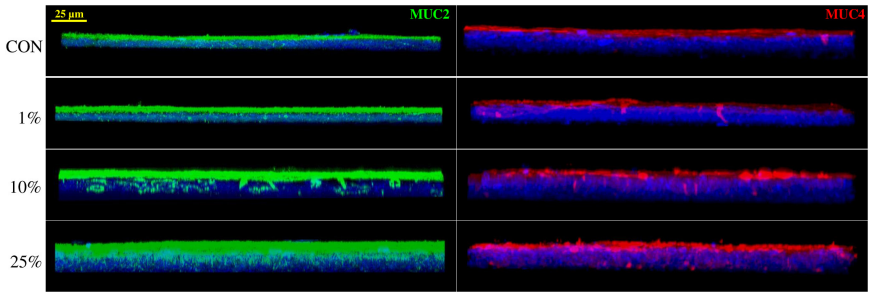

FIGURE 3 iPSC colon organoid monolayers were treated with 1%, 10%, or 25% batch fermentation supernatant (BF). Mucin 2 (MUC2; green) and Mucin 4 (MUC4; red) were analyzed and is shown in the z-plane view. Nuclei are stained with DAPI (blue). Images are representative fields of view at 40X magnification. Images were obtained with Zen Software Version 3.3 (Zeiss; Oberkochen, Germany, https://www.zeiss.com/microscopy/int/products/microscope-software.html)

no differences between 10 and 25%. Overall cell height was also increased at 10 and 25% in MUC2 monolayers compared to CON (1.2-fold; $p < 0.05$; Table 2), however MUC4 was not different. Pyroptosis marker caspase-1 (CASP1) was lightly present as seen by immunofluorescence in all samples, including CON. However, increased signal was observed at 10, and especially 25% (Figure S1). Compared to CON, 1, 10, and 25% BF increased CASP1+ cells (0, 0.16, 0.33, 0.46%, respectively; $p < 0.05$).

3.2.3 | Scanning electron microscopy

SEM is capable of high-resolution images which show ultrastructure of the apical brush border of the intestine as well as extracellular surfaces in general. Images taken at 5000X show more of the general extracellular surface structure while images at 20,000X show more specific features of the brush border such as individual microvilli and microvillar bundles (Figure 4).

TABLE 2 Cell and mucus heights

	CON	1%	10%	25%
MUC2				
Mucus height	$8.52^{a} \pm 0.38$	$9.04^{a} \pm 0.56$	$15.61^{b} \pm 1.33$	$14.08^{b} \pm 0.72$
Cell height	$17.72^{a} \pm 1.95$	$17.91^{ab} \pm 0.74$	$22.90^{c} \pm 1.49$	$20.62^{b} \pm 1.16$
MUC4				
Mucus height	$9.17^{a} \pm 1.23$	$9.03^{a} \pm 0.92$	$14.17^{b} \pm 0.19$	$14.09^{b} \pm 0.71$
Cell height	18.68 ± 0.97	18.13 ± 0.67	20.77 ± 1.18	20.94 ± 2.27

Note: $p^{a,b,c} < 0.05$, $n = 6$.

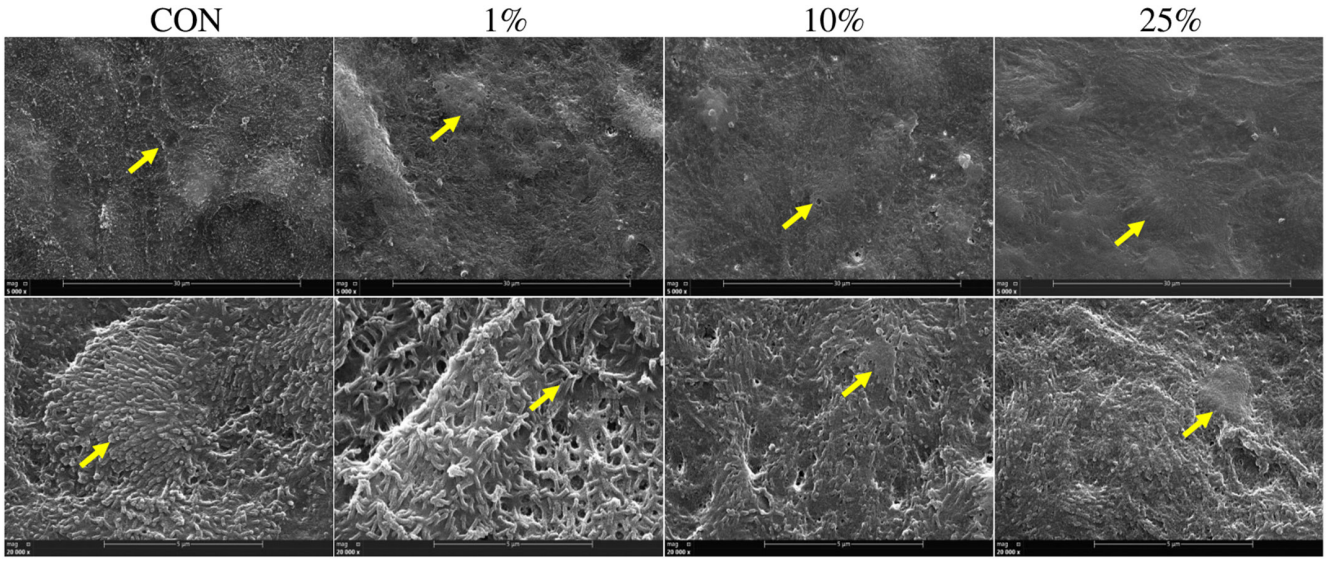

FIGURE 4 iPSC colon organoid monolayers were treated with 1%, 10%, or 25% batch fermentation supernatant (BF) for 72 h. Scanning electron microscopy imaging was conducted and images were taken at 5000 and 20,000X. Images are representative fields of view. Arrows point to suspected mucin clusters

Colon organoid monolayers were observed to have a robust layer of mucin and densely packed microvilli-like structures, with higher percentage FS-treated cells having pockets of mucin formed compared to untreated (Figure 4). This observation is in line with the thickening of the mucosal layer as noted in Figure 3. Colon organoid differentiation with increasing percentage of FS was characterized by noticeably enhanced brush border organization including more dense microvilli at high magnification, but also an increase in the characteristic honeycombing pattern which accompanies differentiation. SEM further showed that the apical surface is covered with a thick layer of mucus which appeared to "flatten" microvilli and make the honeycomb pattern difficult to observe.

3.2.4 | Secreted proteins

IL-1β, IL-10, IL-17A, and IL-18 were increased at 10 and 25% compared to CON and 1% ($p < 0.05$; Table 3). The same markers were also increased significantly at 25% compared to 10%. IL-8, TNF-α, and MCP-1 were significantly increased at 10% FS treatment compared to CON, 1%, and 25%. IL-21, IL-23, CD14, REG3A, and CASP3 were not statistically different between treatments ($p > 0.05$; Table 3). IL-6 was significantly decreased at 25% compared to CON and 10%, but not 1%. Interestingly, IFN-γ was significantly decreased more than 10-fold at 1, 10, and 25% compared to CON ($p < 0.05$; Table 3).

3.2.5 | Barrier function

Supernatant from batch fermentation elicited a concentration-dependent increase in transepithelial electrical resistance (TER) over the 72 h experimental period with significant separation at the 72 h time point ($p < 0.05$; Figure 5A). In the 25% group, TER increased more than two-fold compared to CON. Monolayers treated with 25% all reached greater than 1000 Ω, with some wells reaching over 1700 Ω.

TABLE 3 Inflammatory marker concentrations in iPSC colon organoid media, pg/mL

	IL-1β	IL-6	IL-8	IL-10	IL-17A	IL-18	IL-21	IL-23	TNFα	IFNγ	CD14	REG3A	CASP3	MCP-1
CON	0.18^{a}	5.16^{ab}	165.4^{a}	0.06	0.32^{a}	0.64^{a}	13.18	24.94	4.75^{a}	4.47^{a}	19.33	2.96	7990	22.2^{a}
1%	0.33^{a}	3.70^{bc}	166.6^{a}	0.07	0.35^{a}	0.75^{a}	12.96	23.52	4.70^{a}	0.77^{b}	19.63	3.22	6594	88.7^{a}
10%	1.68^{b}	5.50^{a}	208.5^{b}	0.11	1.79^{b}	3.38^{b}	14.72	34.91	5.39^{b}	0.25^{b}	21.97	3.53	8047	319.5^{b}
25%	2.65^{c}	3.57^{c}	172.2^{a}	0.26	4.56^{c}	9.06^{c}	13.27	19.94	4.94^{ab}	0.26^{b}	19.66	2.92	8393	4.87^{a}
SE	0.08	0.50	6.48	0.01	0.16	0.26	0.94	3.44	0.06	0.11	0.85	0.11	173.3	34.5

Note: Organoids were treated with 1%, 10%, or 25% batch fermentation supernatant (BF) for 72 h.

Abbreviation: SE, standard error.

$^{a,b,c}p < 0.05$, $n = 6$.

3.3 | Continuous multistage fermentation

3.3.1 | mRNA expression

Within clarified supernatants (10%) derived from continuous culture, *LGR5* gene expression was decreased in all treatments, with the largest decrease observed in TC-treated organoids ($p < 0.05$; Figure 6). *ALPI* expression was increased 2.7 and 2.2-fold in TC and DC-treated samples compared to CON while *CHGA* expression was increased by all treatments equally ($p < 0.05$), while *MCT1* was only significantly increased by AC and DC treatments. There was no statistical difference in *LYZ* expression ($p > 0.05$). Expression of *MUC2* was only affected by treatment with TC supernatants which caused a nearly 50% reduction in expression ($p < 0.05$). *MUC4* was increased by all treatments compared to CON, however, TC and DC-treated samples had the largest effect (7.3-and 8.6-fold increase, respectively). *TFF3* was decreased similarly across treatments compared to CON ($p < 0.05$). *MUC5A* expression was significantly decreased in organoids treated with 10% TC supernatants ($p < 0.05$), while expression in those treated with DC was unaltered ($p > 0.05$) compared to CON. There was no effect of treatments on *MUC3A* expression ($p > 0.05$; Figure 5). *TLR2* gene expression was only altered in AC-treated organoids compared to CON (1.5-fold increase; $p < 0.05$). Interestingly, *TLR3* was increased due to AC and DC treatments as compared to CON (1.6-fold; $p < 0.05$), but significantly decreased due to TC treatment ($p < 0.05$) as compared to all other treatments. *TLR4* expression was only increased in AC-treated organoids (1.6-fold; $p < 0.05$) compared to CON, TC, and DC treatments. *TLR5* expression pattern was significantly increased in all treatments compared to CON; however, AC and DC-treated samples were also increased compared to TC (4.1-fold vs. 2.6-fold; $p < 0.05$). *CLDN3* was significantly increased in all treatments compared to CON ($p < 0.05$), however DC-treated organoids had the greatest increase in gene expression (2.9-fold; $p < 0.05$). *TJP1* and *CDH1* gene expression were only significantly affected by DC treatment (1.7-fold increase relative to CON; $p < 0.05$). There was no difference across treatments in *OCLN* expression ($p > 0.05$).

3.3.2 | Immunofluorescence

Protein expression via immunofluorescent intensity of ZO1 was statistically increased in all treatments compared to CON ($p < 0.05$; Figure 7). CLDN3 expression was increased due to all continuous batch treatments ($p < 0.05$); however, AC was statistically higher than TC and DC-treated samples ($p < 0.05$; Figure 7). Compared to CON,

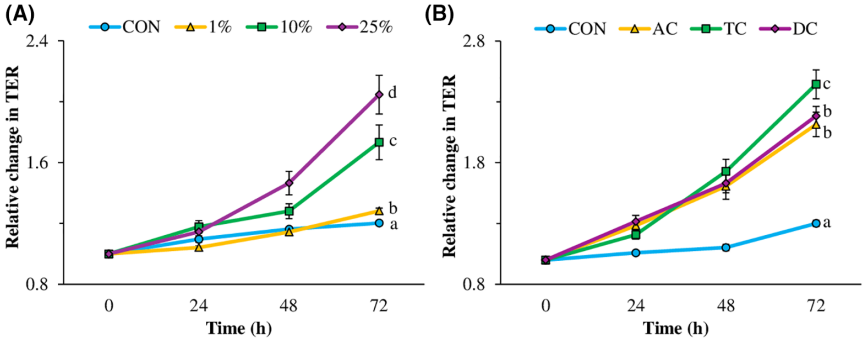

FIGURE 5 iPSC colon organoid monolayers were treated with (A) 1%, 10%, or 25% batch fermentation supernatant (BF) or (B) 10% multistage FS from the ascending (AC), transverse (TC), or descending (DC) colon for 72 h. Transepithelial electrical resistance was measured every 24 h for the duration of the experiment. Different letters represent differences among treatments at 72 h, $n = 8$. Average starting TER was 575 Ω

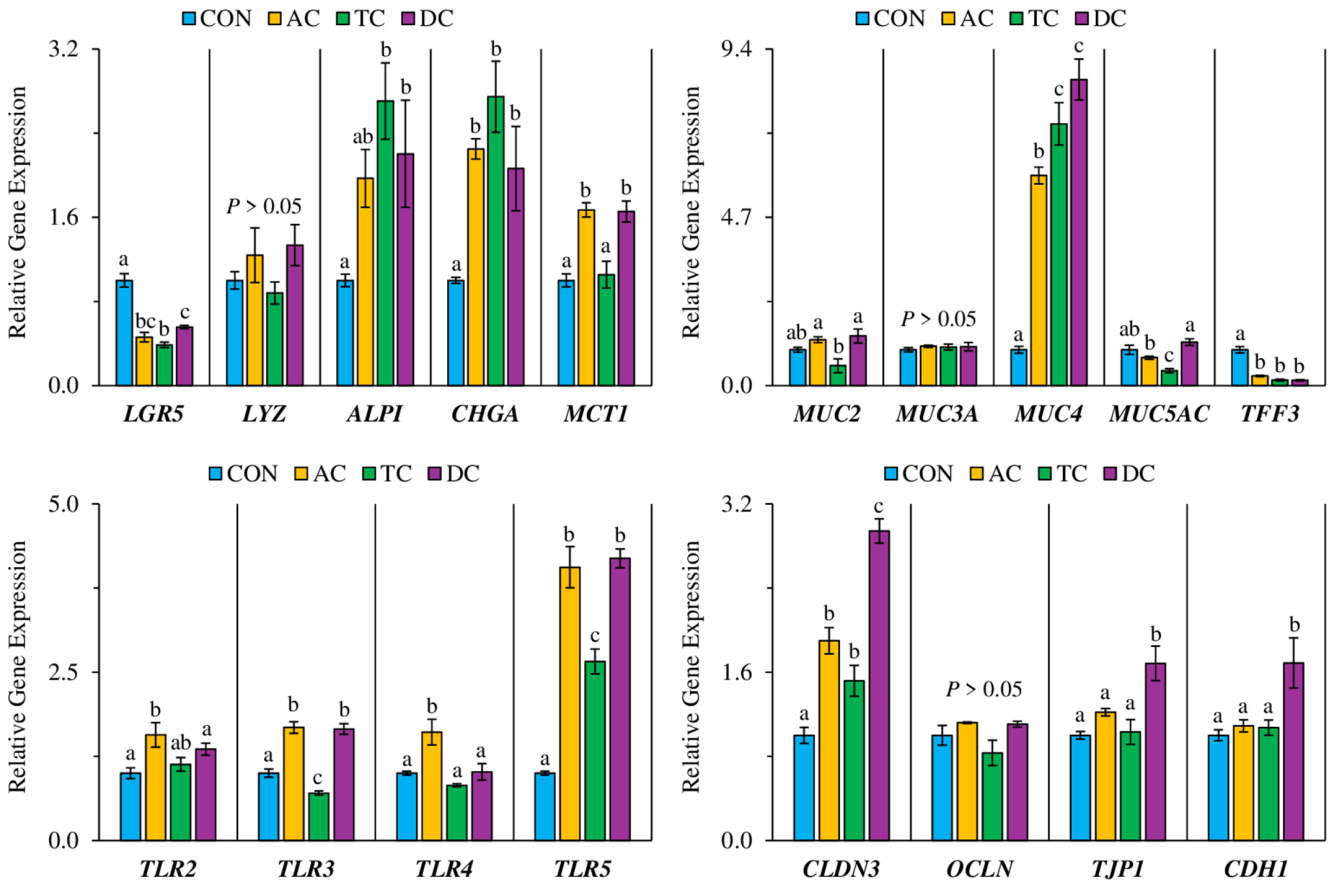

FIGURE 6 iPSC colon organoid monolayers were treated with 10% multistage fermentation supernatant from the ascending (AC), transverse (TC), or descending colon (DC) for 72 h. mRNA expression of several markers including leucine-rich (*LGR5*), lysozyme (*LYZ*), alkaline phosphatase (*ALPI*), chromogranin A (*CHGA*), monocarboxylate transporter 1 (*MCT1*), mucin-2 (*MUC2*), mucin-3A (*MUC3A*), mucin-4 (*MUC4*), mucin-5 AC (*MUC5AC*), trefoil factor 3 (*TFF3*), Toll-like receptor 2 (*TLR2*), Toll-like receptor 3 (*TLR3*), Toll-like receptor 4 (*TLR4*), Toll-like receptor 5 (*TLR5*), claudin-3 (*CLDN3*), occludin (*OCLN*), tight junction protein 1 (*TJP1*), and cadherin 1 (*CDH1*) were analyzed and compared to controls which are set to 1.0. Different letters represent differences among treatments within each gene, $n = 6$

OCLN expression was statistically increased in AC-treated samples but not DC- or TC-treated samples. An additional TJ protein, Claudin-7 (CLDN7) also appeared to follow a similar trend to CLDN3 (Figure S3). Similarly to batch fermentation, both MUC2 and MUC4 were present in treated monolayers (Figure 8). MUC2 and MUC4 were increased in all treatments (1.6-fold; $p < 0.05$). However, AC-treated cells were significantly higher than both TC, and

DC-treated cells ($p < 0.05$; Table 4). Monolayer height in MUC2 and MUC2 stained monolayers was not increased due to treatment ($p > 0.05$; Table 4). Pyroptosis marker caspase-1 (CASP1) was lightly present as seen by immunofluorescence in all samples, including CON. However, increased signal was observed in DC-treated samples (Figure S2). Compared to CON, AC, TC, and DC-treated cells exhibited a significant increase in CASP1+ cells (0, 0.38, 0.33, and 0.70%, respectively; $p < 0.05$). However, DC-treated samples exhibited a nearly twofold increase in CASP1+ cells compared to AC- and TC-treated cells (0.35 vs. 0.70%; $p < 0.05$).

3.3.3 | Scanning electron microscopy

All treatments showed a robust layer of mucus compared to CON, with no discernable differences between FS treatments (Figure 9). Results were similar to that observed from batch-derived supernatants.

3.3.4 | Secreted proteins

IL-1β, IL-8, IL-10, IL-17A, IL-18, IL-21, IL-23, TNFα, IFNγ, CD14, and REG3A were all significantly elevated in DC-treated samples only compared to CON and other FS treatments ($p < 0.05$; Table 5). IL-6 was increased in all treatments compared to CON ($p < 0.05$; Table 5), however was increased highest in DC-treated samples. CASP3 and MCP-1 were not statistically different between treatments ($p > 0.05$; Table 5).

3.3.5 | Barrier function

All organoids were treated with 10% FS from different colonic regions. By 72 h, TER in all treatments was significantly increased twofold compared to CON ($P < 0.05$; Figure 5B). In addition, TER in TC-treated samples was significantly increased compared to DC at 72 h. ($p < 0.05$).

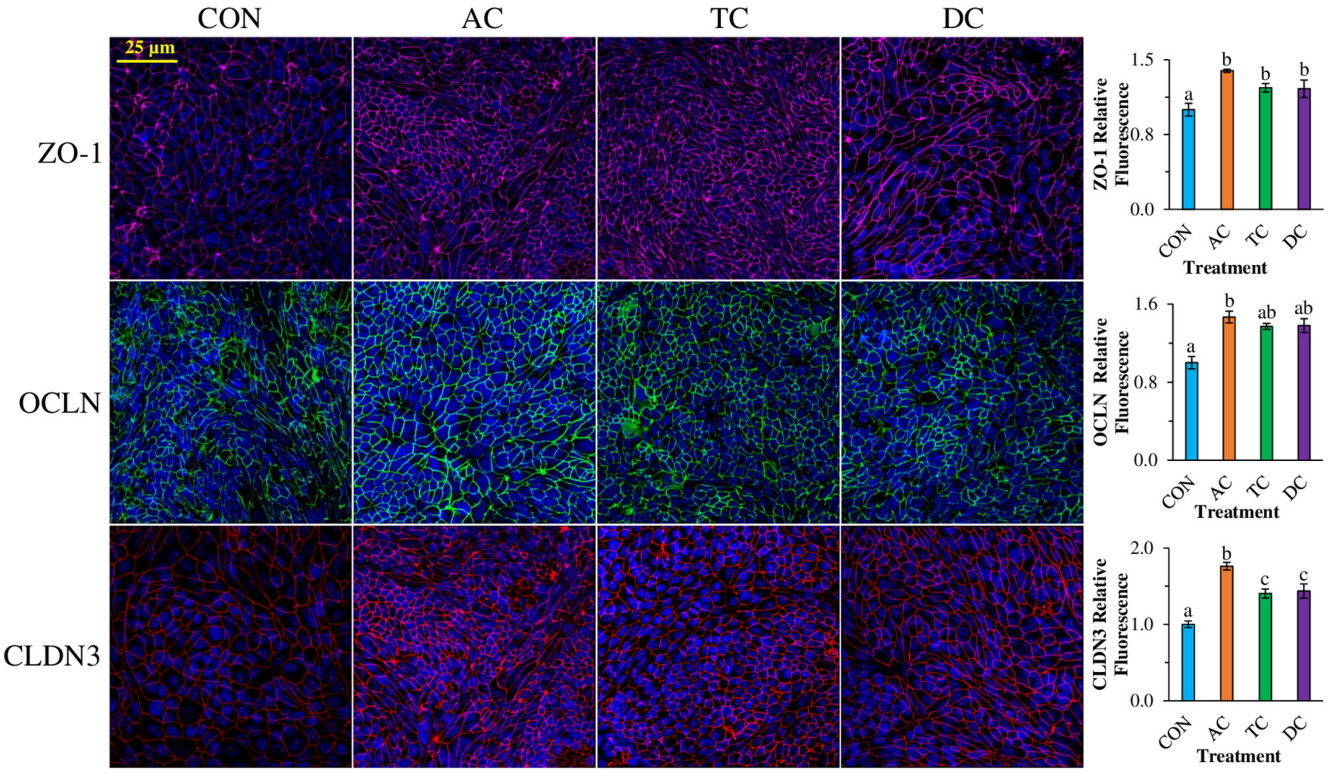

FIGURE 7 iPSC colon organoid monolayers were treated with 10% multistage fermentation supernatant from the ascending (AC), transverse (TC), descending (DC) colon for 72 h. Tight junction proteins zonula occluden 1 (ZO-1; red), and claudin 3 (CLDN3; red) were analyzed and relative fluorescent intensity calculated. Nuclei are stained with DAPI (blue). Images are representative fields of view at 40X magnification. Different letters represent differences among treatments, $n = 6$. Images were obtained with Zen Software Version 3.3 (Zeiss; Oberkochen, Germany, https://www.zeiss.com/microscopy/int/products/microscope-software.html)

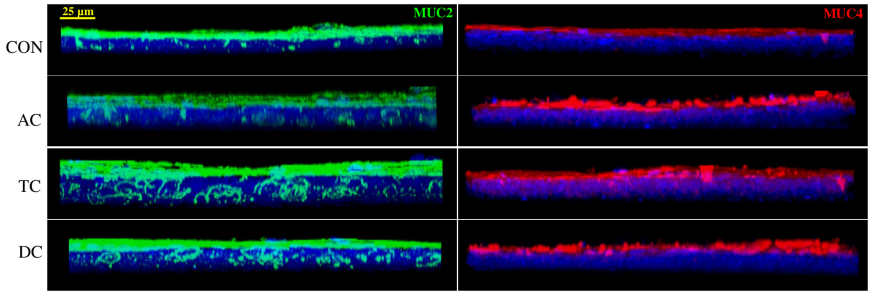

FIGURE 8 iPSC colon organoid monolayers were treated with 10% multistage fermentation supernatant from the ascending (AC), transverse (TC), or descending colon (DC) for 72 h. Mucin 2 (MUC2; green) and mucin 4 (MUC4; red) were analyzed and is shown in the z-plane. Nuclei are stained with DAPI (blue). Images are representative fields of view at 40X magnification. Images were obtained with Zen Software Version 3.3 (Zeiss; Oberkochen, Germany, https://www.zeiss.com/microscopy/int/products/microscope-software.html)

TABLE 4 Cell and mucus heights

	CON	AC	TC	DC
MUC2				
Mucus height	$8.52^{a} \pm 0.39$	$16.33^{c} \pm 0.88$	$14.67^{b} \pm 1.09$	$15.33^{b} \pm 0.88$
Cell height	17.64 ± 1.54	22.25 ± 2.17	20.29 ± 1.11	20.82 ± 1.60
MUC4	$9.17^{a} \pm 1.23$	$18.04^{c} \pm 0.80$	$14.56^{b} \pm 1.11$	$13.62^{b} \pm 1.35$
Mucus height	17.93 ± 0.78	19.98 ± 2.34	20.04 ± 1.27	19.67 ± 2.16
Cell height				

Note: $p^{a,b,c} < 0.05$, $n = 6$.

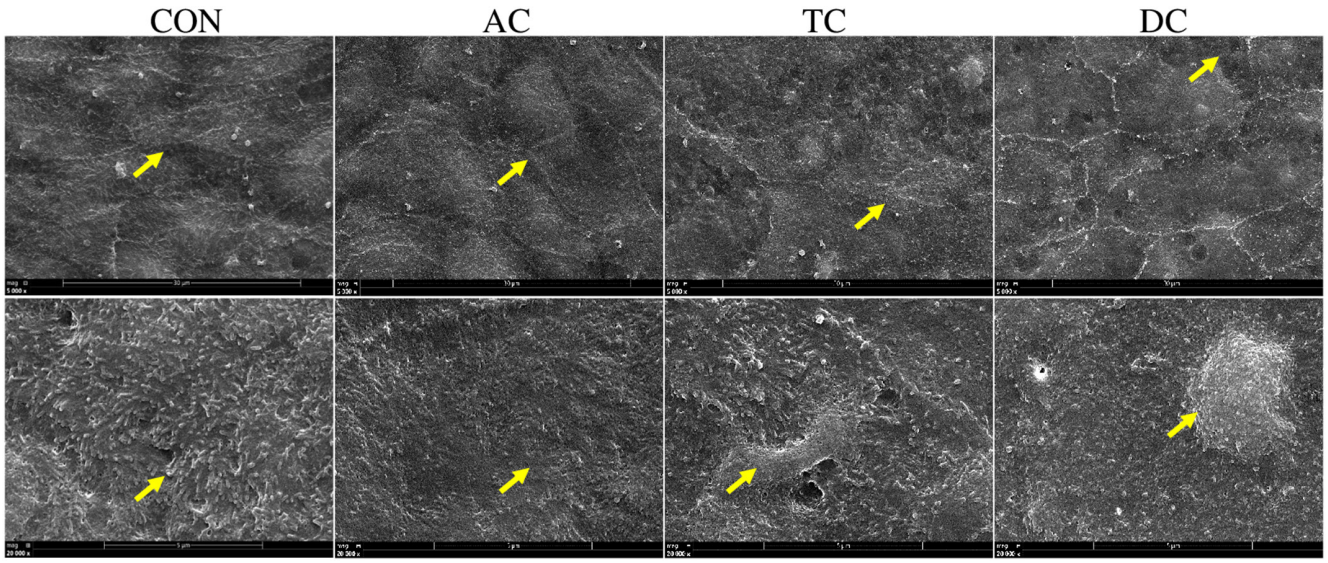

FIGURE 9 iPSC colon organoid monolayers were treated with 10% of multistage fermentation supernatant from the ascending (AC), transverse (TC), or descending (DC) colon for 72 h. Scanning electron microscopy imaging was conducted and images were taken at 5000 and 20,000X. Images are representative fields of view. Arrows point to suspected mucin clusters

3.4 | iPSC characterization

Undifferentiated iPSC colon organoids grown in commercial media displayed a substantial amount of mesenchyme marker Vimentin (VIM; Figure S4) compared to undifferentiated biopsy-derived colon organoids, however VIM was present in both. Both cell lines contained nuclei-specific transcription factor Forkhead Box F1 (FOXF1; Figure S4).

TABLE 5 Inflammatory marker concentrations in iPSC colon organoid media, pg/mL

	IL-1β	IL-6	IL-8	IL-10	IL-17A	IL-18	IL-21	IL-23	TNFα	IFNγ	CD14	REG3A	CASP3	MCP-1
CON	2.28[a]	7.75[a]	140.1[a]	0.89[a]	16.20[a]	13.78[a]	11.70[a]	18.20[a]	1.43[a]	12.37[a]	18.22[a]	9.13[a]	504.2[a]	99.8
AC	2.56[a]	15.28[b]	157.1[a]	1.07[a]	17.50[a]	12.92[a]	12.31[a]	48.85[a]	1.68[a]	18.66[a]	17.20[a]	12.03[a]	977.0[a]	50.5
TC	2.00[a]	13.08[ab]	154.2[a]	0.81[a]	16.68[a]	14.29[a]	12.51[a]	34.03[a]	1.16[a]	8.17[a]	12.88[a]	11.65[a]	466.6[a]	20.8
DC	6.15[b]	27.58[c]	228.7[b]	2.09[b]	23.38[b]	24.09[b]	34.39[b]	114.43[b]	4.49[b]	42.35[b]	27.72[b]	20.09[b]	1696.2[b].	32.9
SE	0.37	1.59	15.52	0.30	0.96	2.06	2.64	9.33	0.86	3.01	3.85	1.35	248.14	16.34

Note: Organoids were treated with 10% multi-stage fermentation supernatant from ascending (AC), transverse (TC), or descending (DC) colon for 72 h.

Abbreviation: SE, standard error.

[a,b,c] $p < 0.05$, $n = 6$.

Several region-specific genes were also analyzed between cell lines. Homeobox Protein CDX-2 (CDX2) was similar between lines and is thought to be evenly expressed across the proximal-distal axis of the colon (Table S2). Prostate, Rectum, and Colon Expressed Gene Protein (PRAC1) and Homeobox Protein Hox-B13 (HOXB13), which are both restricted to distal colon were not present in iPSC colon organoids and were highly expressed in biopsy-derived distal colon organoids (Table S2). Additionally, Carbonic Anhydrase 1 (CA-1) was much more highly expressed in biopsy-derived versus iPSC organoids. Conversely, the sulfate transporter SLC26A2 and apical Na/H exchanger-3 (NHE3; Table S2) were much more highly expressed in iPSC compared to biopsy derived. Taken together, these data suggest that the iPSC represent a more proximal colon region with a present mesenchyme, even after multiple passages.

4 | DISCUSSION

The host–microbe interface is a bi-directional relationship. For example, certain commensal bacteria utilize host-produced mucin as an energy source.[17] On the other hand, the host relies on microbes to break down certain dietary inputs. Metabolism is a key component of biological function, and outcomes of metabolism include metabolites. Microbial metabolites interact directly at the cellular level and affect physiological processes. Metabolites produced by commensal bacteria via the breakdown of dietary inputs include compounds such as SCFA's, BCFA's, protein metabolites, neurotransmitters, bile acid metabolites, hydrogen sulfide, and polyphenol metabolites, among others.[18] SCFA's have been shown to improve mucin secretion and intestinal barrier integrity in a variety of models,[7] while polyphenol and protein metabolites are thought to have potent antioxidant and anti-inflammatory activity.[17] These metabolites have a variety of biological functions ranging from cellular differentiation to barrier protection, and immune system activation.

iPSC models have been rapidly expanding and represent an additional tool to study both development as well as nutrition and host interactions.[19] However, these models have not been fully characterized thus we were interested in utilizing a commercially available iPSC colonoid model and seeing how this line behaved under a monolayer format and with a milieu of microbial metabolites obtained through in vitro fermentation. In our hands the iPSC colon organoid monolayers have some presence of a mesenchyme, indicating a mixed cell population. Both VIM and FOXF1, known mesenchymal markers[20,21] were observed in some capacity. FOXF1is also important for embryonic development[22] and as a mesoderm marker.[23] In

addition, we believe these iPSC cells to be more proximal than distal colon based on several known markers based on previous colonic regional characterization papers.[24–26] iPSC lines have largely been helpful tools for studying development but now are being utilized for disease work as well.[12,13]

In the current study, we have determined that increasing concentrations of FS cause cellular differentiation of human iPSC colon organoid monolayers, such that a more differentiated phenotype is achieved. Mucin is very important for host defense protection of the intestinal epithelium.[27] *MUC2 (*a secreted mucin*)* gene expression was decreased, however, MUC2 mucus height was higher in organoids treated with batch (BF) and in multistage (AC, TC, and DC)-treated samples as compared to control. Gene transcription may be downregulated as a negative feedback loop as mucus production is very high. It is also possible the increased cytokine production observed in several of the FS-treated samples may be in response to stimulation by bacterial metabolites, which could have a negative effect on gene expression (i.e., *MUC2*, *TFF3*). Future experiments could test this hypothesis by culturing colon organoids in an organ-on-a-chip system, simulating flow and washing away cytokines that may be increased and remain in a static system. The mucin layer in FS-treated samples, especially at higher concentrations represents a more robust epithelial defense and is similar in appearance to other published work in colon organoid models.[28] Interestingly, gene expression of *MUC4*, a membrane-bound component of the glycocalyx was highly upregulated due to increased FS exposure. MUC4 is present on both goblet cells and enterocytes but this could be related to differentiation.[29] In the continuous multistage samples, MUC2 was also increased in all colonic domains with few discernible differences between ascending, transverse, and descending colon supernatants. Mucin staining pattern looks similar to that found in human colonoids.[30]

Apical morphology of monolayers has also been shown under a largely proliferative or largely differentiated human colon organoid monolayers where differentiation caused high density of long microvilli with visible secretory granules.[31] To our knowledge, this is the first paper to visualize human iPSC colon organoid monolayers under SEM.

As another important part of the epithelial barrier, tight junctions (TJ), and adherens junctions are part of a larger network of junctional complexes which regulate paracellular permeability between adjacent epithelial cells.[32] These proteins, along with the actin cytoskeleton, control permeability.[33] As TJ proteins are often regulated posttranslationally, we examined these through immunofluorescence. Claudin-3 (CLDN3) is highly expressed in the colon, and helps to tighten epithelial TJ[34] while ZO-1 interacts directly with claudin proteins.[35] Increased barrier integrity is associated with changes in TJ protein expression and distribution, which correlates with functional measures such as transepithelial electrical resistance (TER). Bacterial metabolites have been shown to induce intestinal barrier function maturation by promoting claudin-3 expression and TER.[36,37] In the current study we see a typical sharp honeycomb-like organization of cells at all concentrations of FS, however we observed much higher intensity and more structured organization at 10% and 25% FS. CLDN3 and ZO-1 were located at the usual cell–cell junctions, suggesting enhanced barrier integrity at 10% and 25% FS. As with previous work published in enteroid models,[7] claudin-3 seemed to be the most responsive gene and protein expression wise, whereas occludin and zonula occluden 1 were only responsive at a protein level.

Intestinal barrier function was dramatically increased by increasing FS treatment and TER values reached on average 1400 Ω at 25% FS. This is significantly higher TER than another previously reported undifferentiated iPSC models[38,39] but is comparable to differentiated uninfected biopsy-derived colonoid monolayers.[40]

One of the better understood mechanisms of host–microbe interaction is through the immune system. For example, pattern-recognition receptors (PRR's) help recognize both pathogens and non-pathogens. Toll-like receptors (TLRs) are one of the four sub-families of PRRs[41] and have been found to be expressed on the apical and basolateral sides of several epithelial cell sub-types as well as immune cells.[42] Encouragingly, the distinct TLR expression pattern in epithelial cells is maintained in intestinal organoids, which shows that this expression is not dependent on immune cells nor a present microbiota. In addition, prior studies have shown expression of *TLR2*, *TLR4*, and *TLR5* in colon organoids.[42] Lysozyme, which in the small intestine and ascending colon is a Paneth cell marker[43,44] and antimicrobial peptide was largely unaltered due to treatment but was expressed in the iPSC colon organoids, suggesting a regionality to the iPSC model. In fact, other induced organoid models have been shown to express more proximal colonic markers including CDX2, and LYZ.[19] Interestingly, secreted interleukins were largely altered at 10 and 25% FS, and in the DC continuous multistage experiment. These data were also corroborated by caspase-1 expression which is known as an inflammatory caspase involved in the inflammasome. It is responsible for activation of highly pro-inflammatory cytokines IL-1B and IL-18 and initiates pyroptosis, which is associated with the antimicrobial response as well as regulation

of cellular differentiation. IL-18 specifically is involved in maintenance of intestinal barrier function through mucus production.[45]

The main products of colonic fermentation are SCFA's,[46,47] and when sources are unavailable, protein fermentation can contribute to the SCFA pool, but largely gives rise to BCFAs.[48] In the current study, FS samples contained high total SCFA concentrations with a 60:20:20 ratio, with acetate being highest. In the continuous multi-stage experiment, total SCFA's increased from AC to DC, with increased acetate, and propionate, but relatively no change in butyrate, although butyrate was found in highest concentration in all three. In vitro fermentation conditions and SCFA concentrations were relatively similar to those found in previous batch[49] as well as continuous[50] in vitro fermentation studies. Those studies also showed markers of protein metabolism p-Cresol and ammonia and determined that the main proteolytic regions of the colon are TC and DC. Our group has previously shown that single SCFA's at higher concentrations (10 mM) inhibit proliferation while enhancing barrier function in an organoid model.[7]

In conclusion, the microbial metabolite milieu produced via in vitro fermentation when diluted with cell media has a significant effect on intestinal barrier function and other epithelial cell markers. This includes positive changes in markers of epithelial differentiation, mucin host defense, pattern-recognition receptor expression, and epithelial barrier integrity. Validation of the host-in vitro integration model will be expanded upon in the future using real time exposures so that cells are exposed as bacteria are actively fermenting, as well as full characterization of the associated metabolome. In addition, this model can be used to study nutritional interventions under military-relevant, or other types of stress or disease.

ACKNOWLEDGMENTS

The authors would like to acknowledge and thank Gianna Ahnrud and David Ziegler of the Combat Capabilities Development Command Soldier Center Imaging Facility for Scanning Electron Microscopy Images. The authors would also like to acknowledge and thank Katherine Kensil of the Combat Capabilities Development Command Soldier Center Analytical Chemistry Laboratory for analyzing SCFA and BCFA profiles. Also, Steven Arcidiacono and Ida Pantoja-Feliciano for support on continuous fermentation. The authors would like to acknowledge Dana M. van Sambeek of the Combat Capabilities Development Command Soldier Center Integrated Physiology Laboratory for his assistance with editing and methods optimization. The authors would also like to acknowledge Dr. David Breault of Boston Children's Hospital and Harvard for use of biopsy-derived colon organoids used for characterization comparison.

CONFLICT OF INTEREST

N/A

AUTHOR CONTRIBUTIONS

GJW helped edit manuscript and conducted sample analysis and experiments, LAD helped write and edit manuscript, provided fermentation experimental design, samples and methods, and conducted fermentation experiments, JWS helped edit manuscript and provided fermentation experimental design, samples, and methods, SCP designed, wrote, conducted experiments, conducted sample analysis, analyzed data, and edited the manuscript.

DISCLAIMER

The opinions or assertions contained herein are the private views of the author(s) and are not to be construed as official or as reflecting the views of the Army or the Department of Defense. Citation of commercial organizations or trade names in this report does not constitute an official Department of the Army endorsement or approval of the products or services of these organizations. Opinions, interpretations, conclusions, and recommendations are those of the authors and are not necessarily endorsed by the US Army.

ORCID

Sarah C. Pearce https://orcid.org/0000-0003-4822-6896

REFERENCES

1. Hill DR, Spence JR. Gastrointestinal organoids: understanding the molecular basis of the host-microbe Interface. *Cell Mol Gastroenterol Hepatol*. 2017;3:138-149.
2. Villageliu DN, Rasmussen S, Lyte M. A microbial endocrinology-based simulated small intestinal medium for the evaluation of neurochemical production by gut microbiota. *FEMS Microbiol Ecol*. 2018;94(7).
3. Nissen L, Casciano F, Gianotti A. Intestinal fermentation in vitro models to study food-induced gut microbiota shift: an updated review. *FEMS Microbiol Lett*. 2020;367:367.
4. Moon JS, Li L, Bang J, Han NS. Application of in vitro gut fermentation models to food components: a review. *Food Sci Biotechnol*. 2016;25:1-7.
5. Pearce SC, Coia HG, Karl JP, Pantoja-Feliciano IG, Zachos NC, Racicot K. Intestinal in vitro and ex vivo models to study host-microbiome interactions and acute stressors. *Front Physiol*. 2018;9:1584.
6. Sontheimer-Phelps A, Chou DB, Tovaglieri A, et al. Human colon-on-a-Chip enables continuous In vitro analysis of colon mucus layer accumulation and physiology. *Cell Mol Gastroenterol Hepatol*. 2020;9:507-526.
7. Pearce SC, Weber GJ, van Sambeek DM, Soares JW, Racicot K, Breault DT. Intestinal enteroids recapitulate the effects of

short-chain fatty acids on the intestinal epithelium. *PLoS ONE*. 2020;15:e0230231.
8. Foulke-Abel J, In J, Yin J, et al. Human enteroids as a model of upper small intestinal ion transport physiology and pathophysiology. *Gastroenterology*. 2016;150:638-649.e638.
9. Kishida K, Pearce SC, Yu S, Gao N, Ferraris RP. Nutrient sensing by absorptive and secretory progenies of small intestinal stem cells. *Am J Physiol Gastrointest Liver Physiol*. 2017;312:G592-G605.
10. Wang Y, DiSalvo M, Gunasekara DB, et al. Self-renewing monolayer of primary colonic or rectal epithelial cells. *Cell Mol Gastroenterol Hepatol*. 2017;4:165-182.e167.
11. Kozuka K, He Y, Koo-McCoy S, et al. Development and characterization of a human and mouse intestinal epithelial cell monolayer platform. *Stem Cell Reports*. 2017;9:1976-1990.
12. Múnera JO, Sundaram N, Rankin SA, et al. Differentiation of human pluripotent stem cells into colonic organoids via transient activation of BMP signaling. *Cell Stem Cell*. 2017;21:51-64.e56.
13. Spence JR, Mayhew CN, Rankin SA, et al. Directed differentiation of human pluripotent stem cells into intestinal tissue in vitro. *Nature*. 2011;470:105-109.
14. Pantoja-Feliciano IG, Soares JW, Doherty LA, et al. Acute stressor alters inter-species microbial competition for resistant starch-supplemented medium. *Gut Microbes*. 2019;10:439-446.
15. Zhang X, Zhao Y, Zhang M, et al. Structural changes of gut microbiota during berberine-mediated prevention of obesity and insulin resistance in high-fat diet-fed rats. *PLoS ONE*. 2012;7:e42529.
16. Patrone V, Vajana E, Minuti A, et al. Postoperative changes in fecal bacterial communities and fermentation products in obese patients undergoing Bilio-intestinal bypass. *Front Microbiol*. 2016;7:200.
17. Wlodarska M, Luo C, Kolde R, et al. Indoleacrylic acid produced by commensal Peptostreptococcus species suppresses inflammation. *Cell Host Microbe*. 2017;22:25-37.e26.
18. McCarville JL, Chen GY, Cuevas VD, Troha K, Ayres JS. Microbiota metabolites in health and disease. *Annu Rev Immunol*. 2020;38:147-170.
19. Mithal A, Capilla A, Heinze D, et al. Generation of mesenchyme free intestinal organoids from human induced pluripotent stem cells. *Nat Commun*. 2020;11:215.
20. Nishina H, Katou-Ichikawa C, Kuramochi M, Izawa T, Kuwamura M, Yamate J. The localization and distribution of cells labeled by a somatic stem cell-recognizing antibody (A3) in rat colon development; possible presence of a new cell type forming the intestinal stem cell niche. *J Toxicol Pathol*. 2019;32:37-48.
21. Madison BB, McKenna LB, Dolson D, Epstein DJ, Kaestner KH. FoxF1 and FoxL1 link hedgehog signaling and the control of epithelial proliferation in the developing stomach and intestine. *J Biol Chem*. 2009;284:5936-5944.
22. Ren X, Ustiyan V, Pradhan A, et al. FOXF1 transcription factor is required for formation of embryonic vasculature by regulating VEGF signaling in endothelial cells. *Circ Res*. 2014;115:709-720.
23. Yu Q, Kilik U, Holloway EM, et al. Charting human development using a multi-endodermal organ atlas and organoid models. *Cell*. 2021;184:3281-3298.e3222.
24. Glebov OK, Rodriguez LM, Nakahara K, et al. Distinguishing right from left colon by the pattern of gene expression. *Cancer Epidemiol Biomarkers Prev*. 2003;12:755-762.
25. Liu XF, Olsson P, Wolfgang CD, et al. PRAC: a novel small nuclear protein that is specifically expressed in human prostate and colon. *Prostate*. 2001;47:125-131.
26. Tatangelo F, Di Mauro A, Scognamiglio G, et al. Posterior HOX genes and HOTAIR expression in the proximal and distal colon cancer pathogenesis. *J Transl Med*. 2018;16:350.
27. Shirazi T, Longman RJ, Corfield AP, Probert CS. Mucins and inflammatory bowel disease. *Postgrad Med J*. 2000;76:473-478.
28. In JG, Foulke-Abel J, Clarke E, Kovbasnjuk O. Human Colonoid monolayers to study interactions between pathogens, commensals, and host intestinal epithelium. *JoVE*. 2019;9(146):e59357.
29. Lindén SK, Florin THJ, McGuckin MA. Mucin dynamics in intestinal bacterial infection. *PLoS ONE*. 2008;3:e3952.
30. Liu L, Saitz-Rojas W, Smith R, et al. Mucus layer modeling of human colonoids during infection with enteroaggragative *E. coli*. *Sci Rep*. 2020;10:10533.
31. Wang Y, Kim R, Gunasekara DB, et al. Formation of human colonic crypt Array by application of chemical gradients across a shaped epithelial monolayer. *Cell Mol Gastroenterol Hepatol*. 2017;5(2):113-130.
32. Ulluwishewa D, Anderson RC, McNabb WC, Moughan PJ, Wells JM, Roy NC. Regulation of tight junction permeability by intestinal bacteria and dietary components. *J Nutr*. 2011;141:769-776.
33. Buckley A, Turner JR. Cell biology of tight junction barrier regulation and mucosal disease. *Cold Spring Harb Perspect Biol*. 2018;10:a029314.
34. Lu Z, Ding L, Lu Q, Chen Y-H. Claudins in intestines: distribution and functional significance in health and diseases. *Tissue Barriers*. 2013;1:e24978.
35. Itoh M, Furuse M, Morita K, Kubota K, Saitou M, Tsukita S. Direct binding of three tight junction-associated MAGUKs, ZO-1, ZO-2, and ZO-3, with the COOH termini of claudins. *J Cell Biol*. 1999;147:1351-1363.
36. Patel RM, Myers LS, Kurundkar AR, Maheshwari A, Nusrat A, Lin PW. Probiotic bacteria induce maturation of intestinal claudin 3 expression and barrier function. *Am J Pathol*. 2012;180:626-635.
37. Ewaschuk JB, Diaz H, Meddings L, et al. Secreted bioactive factors from Bifidobacterium infantis enhance epithelial cell barrier function. *Am J Physiol Gastrointest Liver Physiol*. 2008;295:G1025-G1034.
38. Yamada S, Kanda Y. Retinoic acid promotes barrier functions in human iPSC-derived intestinal epithelial monolayers. *J Pharmacol Sci*. 2019;140:337-344.
39. Takayama K, Negoro R, Yamashita T, et al. Generation of human iPSC-derived intestinal epithelial cell monolayers by CDX2 transduction. *Cell Mol Gastroenterol Hepatol*. 2019;8:513-526.
40. In J, Foulke-Abel J, Zachos NC, et al. Enterohemorrhagic *Escherichia coli* reduce mucus and intermicrovillar bridges in human stem cell-derived colonoids. *Cell Mol Gastroenterol Hepatol*. 2016;2:48-62.e43.
41. Amarante-Mendes GP, Adjemian S, Branco LM, Zanetti LC, Weinlich R, Bortoluci KR. Pattern recognition receptors and the host cell death molecular machinery. *Front Immunol*. 2018;9(2379).

42. Price AE, Shamardani K, Lugo KA, et al. A map of toll-like receptor expression in the intestinal epithelium reveals distinct spatial, cell type-specific, and temporal patterns. *Immunity*. 2018;49:560-575.e566.
43. Yu S, Balasubramanian I, Laubitz D, et al. Paneth cell-derived lysozyme defines the composition of mucolytic microbiota and the inflammatory tone of the intestine. *Immunity*. 2020;53:398-416.e398.
44. Wang Y, Song W, Wang J, et al. Single-cell transcriptome analysis reveals differential nutrient absorption functions in human intestine. *J Exp Med*. 2020;217(2):e20191130.
45. Rathinam VAK, Chan FK-M. Inflammasome, inflammation, and tissue homeostasis. *Trends Mol Med*. 2018;24:304-318.
46. Oliphant K, Allen-Vercoe E. Macronutrient metabolism by the human gut microbiome: major fermentation by-products and their impact on host health. *Microbiome*. 2019;7:91.
47. Cummings JH, Pomare EW, Branch WJ, Naylor CP, Macfarlane GT. Short chain fatty acids in human large intestine, portal, hepatic and venous blood. *Gut*. 1987;28:1221-1227.
48. Smith EA, Macfarlane GT. Dissimilatory amino acid metabolism in human colonic bacteria. *Anaerobe*. 1997;3:327-337.
49. Wang X, Gibson GR, Costabile A, Sailer M, Theis S, Rastall RA. Prebiotic supplementation of in vitro fecal fermentations inhibits proteolysis by gut bacteria, and host diet shapes gut bacterial metabolism and response to intervention. *Appl Environ Microbiol*. 2019;85(9):e02749-18.
50. Wang X, Gibson GR, Sailer M, Theis S, Rastall RA. Prebiotics inhibit proteolysis by gut bacteria in a host diet-dependent manner: a three-stage continuous in vitro gut model experiment. *Appl Environ Microbiol*. 2020;86(10):e02730-19.

SUPPORTING INFORMATION

Additional supporting information may be found in the online version of the article at the publisher's website.

How to cite this article: Pearce SC, Weber GJ, Doherty LA, Soares JW. Human iPSC colon organoid function is improved by exposure to fecal fermentates. *FASEB BioAdvances*. 2022;4:468–484. doi: 10.1096/fba.2021-00166